

# Acoustic Emission in Plate-Like Structures



Theodore E. Matikas and Dimitrios G. Aggelis

**Abstract** Structural elements commonly obtain plate geometries. This is usual in aeronautics, automotive, naval applications and at the same time becomes more and more common in civil engineering with the expansion in the use of lightweight panels and fibrous media over bulk concrete. Acoustic emission (AE) is typically applied on these geometries yielding excellent results in laboratory and industrial conditions. The plate geometries however, create some specificities compared to bulk geometries. These are mainly related to the conditions of wave propagation since “plate wave dispersion” is exhibited, resulting in strong change of the acoustic signals as they propagate through the material. This influences the received AE waveforms rendering the study of “Lamb waves” of paramount importance in case someone wishes to go into detail in the characterization of plate structures based on their AE behavior. The present chapter offers a firm theoretical basis for guided waves, demonstrates dispersion and tries to examine its influence compared to bulk media from the AE point of view. Several basic applications of AE in plates are given to exhibit the level of the state of the art in laboratory and practice and where it can be further pushed.

**Keywords** Lamb waves · Dispersion · Distortion · Fracture mode characterization · Localization

---

T. E. Matikas (✉)  
Department of Materials Science and Engineering, University of Ioannina, 45110 Ioannina,  
Greece  
e-mail: [matikas@uoi.gr](mailto:matikas@uoi.gr)

D. G. Aggelis  
Department of Mechanics of Materials and Constructions, Vrije Universiteit Brussel, 1050  
Brussels, Belgium  
e-mail: [Dimitrios.aggelis@vub.be](mailto:Dimitrios.aggelis@vub.be)

# 1 Guided Waves in Plate-Like Structures

## 1.1 Rayleigh Waves

If an acoustic wave propagates along the surface of a homogenous plate-like structural element with a wavelength much shorter than the thickness of the plate, such plate can be considered a homogeneous elastic half-space and the wave amplitude decreases exponentially with depth [1–3]. This guided surface wave is called Rayleigh wave. On the free surface these waves eliminate the stresses they produce.

The known Rayleigh wave velocity equation can be derived by considering the displacement potentials:

$$\varphi = A e^{-k \sqrt{1 - \left(\frac{c}{c_L}\right)^2} z} e^{ik(x-ct)} \quad (1)$$

$$\phi = B e^{-k \sqrt{1 - \left(\frac{c}{c_S}\right)^2} z} e^{ik(x-ct)} \quad (2)$$

where  $c = \frac{\omega}{k}$ , with  $\omega$  being the radial frequency and  $k$  the wavenumber,  $c_L$  is the velocity of the longitudinal waves, and  $c_S$  is the velocity of the shear waves, and  $A$  and  $B$  are arbitrary constants.

Using the wave equations for the two potentials (1) and (2) we have,

$$\nabla^2 \varphi = \frac{1}{c_L^2} \ddot{\varphi}, \quad \nabla^2 \phi = \frac{1}{c_S^2} \ddot{\phi} \quad (3)$$

and applying boundary conditions by assuming zero stress at the surface, one can obtain the following characteristic Rayleigh equation:

$$\left(2 - \frac{c_R^2}{c_S^2}\right)^2 - 4 \sqrt{\left(1 - \frac{c_R^2}{c_L^2}\right) \left(1 - \frac{c_R^2}{c_S^2}\right)} = 0 \quad (4)$$

As can be seen from Eq. (4) above, the phase velocity of Rayleigh waves,  $c_R$ , does not depend on the wavenumber  $k$  (i.e., it is frequency independent), therefore the Rayleigh waves are propagated without dispersion. A simple expression of Rayleigh wave velocity based on curve fitting is given by the following equation:

$$c_R \approx c_S \frac{0.87 + 1.12\nu}{1 + \nu} \quad (5)$$

or

$$\frac{c_L}{c_R} = \frac{1 + \nu}{0.87 + 1.12\nu} \sqrt{\frac{2(1 - \nu)}{(1 - 2\nu)}} \tag{6}$$

where  $\nu$  is the Poisson’s ratio, which can be estimated from the longitudinal and shear wave velocities in the material by:

$$\nu \approx \frac{c_L^2 - 2c_S^2}{2(c_L^2 - c_S^2)} \tag{7}$$

For example, for a material with longitudinal and Rayleigh wave velocities  $c_L = 3740$  m/s and  $c_R = 1793$  m/s, respectively, the ratio of the two velocities is  $C_L/C_R = 2.08$ . Considering Eq. (7), the Poisson’s ratio can be calculated,  $\nu = 0.32$ . Given the relations between the elastic moduli (where  $E$  is Young’s modulus and  $G$  is the shear modulus), the longitudinal and shear wave velocities and the material’s density,  $\rho$  (which is assumed here to be concrete  $\rho = 2300$  kg/m<sup>3</sup>):

$$E = \frac{\rho(1 + \nu)(1 - 2\nu)}{1 - \nu} c_L^2 \tag{8}$$

$$G = \rho c_S^2 = \frac{E}{2(1 + \nu)} \tag{9}$$

the two elastic moduli can be easily estimated:  $E \approx 22.5$  GPa and  $G \approx 8.5$  GPa.

The surface acoustic waves have an elliptical particle motion, as shown in Fig. 1, and penetrate the surface of the structure at a depth of around one wavelength, which makes them particularly attractive for characterizing sub-surface damage in materials [4–6]. Generally, the Rayleigh wave velocity is smaller than the respective velocities of longitudinal or shear waves ( $c_R \approx 0.56c_L$  και  $c_R \approx 0.90c_S$ ). The particle motion of a propagating Rayleigh wave is elliptical because the displacements along the  $x$  and  $z$  axes have a phase shift of  $\pi/2$ . Vertical displacement is usually 1.5 times the horizontal component on the surface and the elliptical movement is counterclockwise

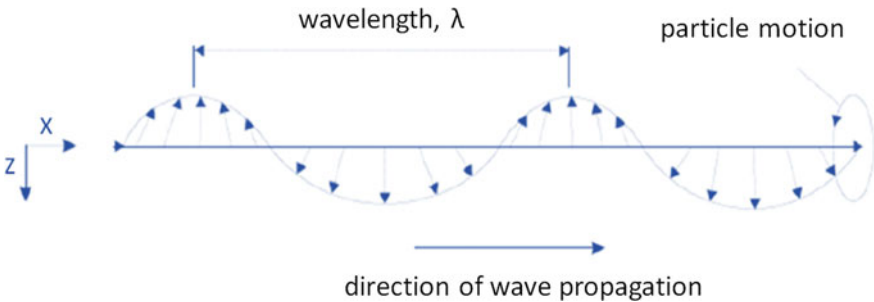


**Fig. 1** Particle motion of a Rayleigh surface wave

along the positive  $x$  direction. At a depth of about 0.2 wavelengths, the direction of the rotation of particles inverts from counterclockwise to clockwise [7, 8].

An important feature of Rayleigh waves is the concentration of energy near the free surface of the material. Therefore, a nondestructive technique based on the use of Rayleigh waves is particularly desirable for the detection of surface defects, as well as of damage located near the surface of the material, such as damage caused by mechanical fatigue [9].

## 1.2 Lamb Waves

A Rayleigh wave will gradually become a plate wave when the plate's thickness becomes comparable to, or smaller than, the wavelength of the surface wave. This occurs at lower frequencies. Guided waves propagating on thin plates with two parallel free surfaces where the stress is zero are called Lamb waves [7–10].

Lamb waves are deformations of a plate-like structure that propagate along the structure. At the axis normal to the plate, they look like standing waves. While in a bulk solid material only two wave modes can exist (longitudinal and shear waves), each propagating at a given velocity (which is a property of the material) independent (at first order) of the frequency, a plate-like structure can support a double infinity of Lamb wave modes, each having a frequency dependent wave speed. Lamb waves do not only exhibit dispersion, but they also have multiple velocity values for a given frequency [11]. The different wave velocities correspond to an infinite number of different Lamb wave propagation modes, which are divided into symmetric (S) and antisymmetric (A) [12–14].

The symmetric modes of wave propagation [15], are also called longitudinal modes, since the mean displacement along the thickness of the plate is in the longitudinal direction (see Fig. 2).

On the contrary, the antisymmetric modes of propagation, are also called bending modes, since the mean displacement along the thickness of the plate is in the transverse direction (see Fig. 3). The infinite number of propagation modes exists for a particular combination of plate thickness and ultrasonic frequency, and each mode has its own phase velocity.

In classical ultrasonic studies Lamb waves are generated using ultrasonic transducers with a proper incoming wave angle [16, 17]. The propagation characteristics

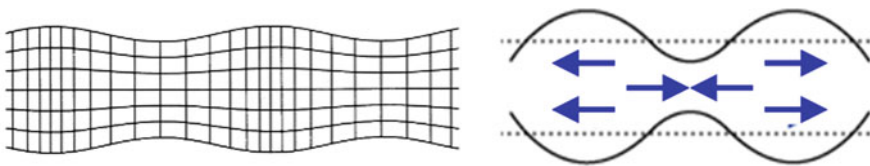


**Fig. 2** Symmetric modes of plate wave propagation (Lamb wave)

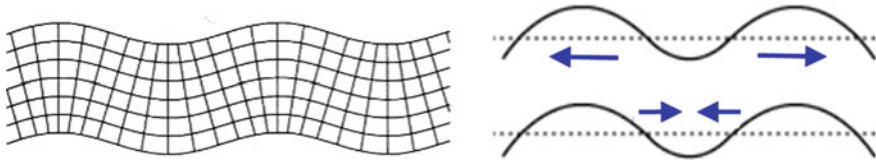


**Fig. 3** Antisymmetric modes of plate wave propagation (Lamb wave)

of Lamb waves are described using dispersion curves based on the phase velocity of the plate as a function of the ultrasonic frequency—plate thickness product [18, 19]. The various dispersion modes are named S0, A0, S1, A1, etc., depending on whether the propagation mode is symmetric or antisymmetric. Figure 4 shows the phase velocity dispersion curves for a thin aluminum plate.

If the frequency of plate waves is high enough so that the wavelength is much shorter than the plate thickness, these waves will have a velocity equal to the Rayleigh wave velocity of the material propagating in a half-space. In this case, a combination of a symmetric and an antisymmetric mode of equal amplitudes will result in a single Rayleigh wave propagating on either side of the plate. The shorter is the wavelength, the closer is the velocity and the polarization of Lamb waves to the Rayleigh wave limit.

Although the dispersion diagrams are relatively complex, they can be simplified using the incoming wave angle to determine the main Lamb wave mode to be generated [20–24]. A particular Lamb wave mode can be produced if the phase velocity of the incident longitudinal wave equals the phase velocity of that particular mode of

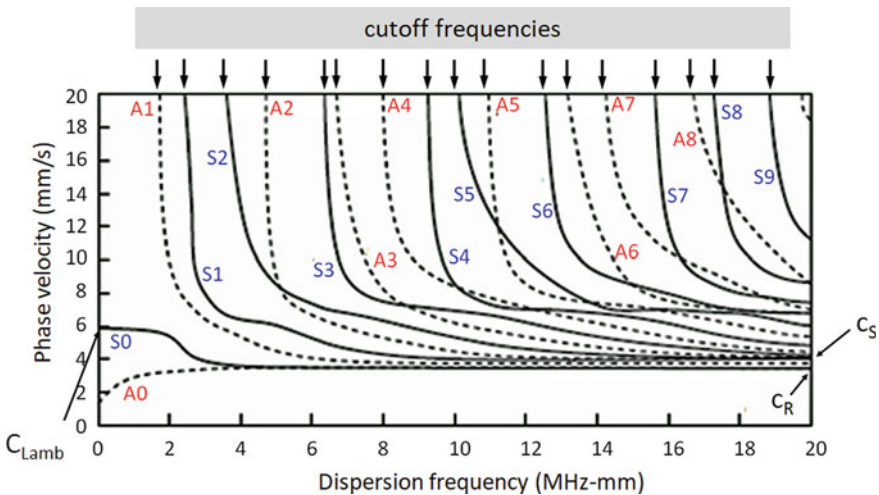


**Fig. 4** Phase velocity dispersion curves for a thin aluminum plate

Lamb wave. Lamb waves are extremely useful for detecting cracks in materials with thin sheet or thin plate geometry, as well as in tubular structures [25], while their study is essential in acoustic emission studies in plate geometries as will be seen.

### 1.3 Other Types of Guided Waves

There are other types of guided waves in plate-like structures that can be of interest for nondestructive testing of materials. These types are briefly mentioned for completeness and are classified according to the structure in which they are propagated, which is called a waveguide. Below are some examples of these types of guided waves.

#### 1.3.1 Love Waves

Love waves are dispersive surface waves resultant from horizontally polarized shear waves. Love waves propagate in solids with velocities varying with depth. They cannot occur in a homogenous half-space. The simplest case in which a quantitative analysis of Love wave propagation can be performed is a thin solid layer (coating) covering an elastic half-space [26]. This type of waves can find important applications in nondestructive testing of coatings and layered structures, including nanocomposites with thin films. These waves are observed when there is a low velocity layer overlying a higher velocity substrate material. Love waves are slower than longitudinal and shear waves, but they propagate with a higher velocity than Rayleigh waves.

Generally, a surface Love wave is described by function  $g(z)$  which depends on depth, with solutions that are exponential functions of depth.

$$g(z) = Ae^{k_L z} + Be^{-k_L z} \quad (10)$$

where

$$k_{LV}^2 = k^2 \left( 1 - \frac{c_{LV}^2}{c_S^2} \right) \quad (11)$$

and  $c_{LV}$  is the Love wave velocity.

Note that one of the solutions increases exponentially with depth, which was eliminated in the case of Rayleigh surface waves.

Since the condition for a surface wave is the displacement to decrease exponentially with depth in the elastic half-space, then  $k_{LV}$  in the substrate material is real and positive. Hence, from Eq. (11),  $c_{LV} = \omega/k$  is lower than the shear wave velocity in the half space  $c_S$ .

For a given ultrasonic frequency a multi-mode solution for the Love wave propagation is obtained, each mode with a different velocity. A finite number of solutions for the Love wave velocity exist, depending on the frequency, the thickness of the coating layer, and the densities and shear wave velocities of the coating and the substrate.

### 1.3.2 Interface Waves in Multilayered Plates

Stoneley waves are guided interface waves propagating along the interface between two solid media [27, 28]. In case of a fluid–solid interface, Scholte’s waves propagate [29]. The interface waves have a maximum intensity at the interface, while it drops exponentially far from it. The existence and propagation of non-attenuative interface waves depends on the interface condition and the combination of properties of the two adjacent materials. Expanding the study of interface waves from the simple two half-space consideration to multilayered structures with  $N$  number of interfaces can find applications in nondestructive testing of structures for a variety of engineering fields for detecting interface defects.

Different types of elastic waves can be propagated in multilayered plates, such as bulk waves, Rayleigh waves, and interface waves. The propagation of bulk waves in such media are characterized by the number of possible modes in a frequency range, the complexity for exciting only one mode in the multilayered plate and significant distortion of the waveform. Rayleigh waves are guided waves propagating along the air–solid interface.

In order to ensure that the layers are relatively thick compared to the wavelength, and hence are equivalent to half-spaces for the induced Rayleigh wave, high frequencies are used. To experimentally distinguish the interfaces waves from other types of waves propagated in an multilayered medium it is necessary to recognize the typical features of them. First, at a given interface, an interface wave can only occur at a single mode. If there are  $N$  interfaces in a multilayered plate, there will exist  $N$  modes of the interface wave. Also, at high ultrasonic frequencies, the group velocity converges to an exact value that corresponds to the group velocity of the true Stoneley wave mode [30].

As there are many possible modes with significant wave distortion propagating in a multilayered plate within a high frequency range, there is a difficulty to precisely excite only a single mode in the structure. A way to generate interface waves is to use surface wave transducers instead of oblique incidence or interdigital transducers used for bulk waves [30].

The characteristic equation of a multilayered plate with  $N$  layers can be obtained in determinant form considering the potential functions of the longitudinal and shear waves in  $n$ th layer.

The displacement field of the  $n$ th layer has to satisfy Navier’s equation of motion. This displacement field is decomposed into two components (longitudinal and shear waves). Taking into account that the Stoneley wave energy should concentrate at the interfaces and decreases exponentially far from these interfaces, the potential

functions for the longitudinal wave ( $\varphi$ ) and for the shear wave ( $\psi$ ) in every layer can be written in the form:

For layers  $n = 2, \dots (N - 1)$

$$\varphi = \{Ae^{-ka_n(z-d_{n-1})} + Be^{ka_n(z-d_{n-1})}\}e^{i(kx-\omega t)} \quad (12)$$

$$\psi = \{Ce^{-kb_n(z-d_{n-1})} + De^{kb_n(z-d_{n-1})}\}e^{i(kx-\omega t)} \quad (13)$$

where, A, B, C, D are unknown coefficients, k is the real wavenumber, d indicates the thickness of the respective layer, and  $a_n^2 = 1 - \frac{c^2}{c_L^2}$ ,  $b_n^2 = 1 - \frac{c^2}{c_S^2}$  (c is the phase velocity of Stoneley waves,  $c_L$  and  $c_S$  are the longitudinal and shear wave velocities, respectively).

For  $n = 1$  there is only the second term in Eqs. (12) and (13), and  $d = 0$ , while for  $n = N$  there is only the first term in Eqs. (12) and (13).

The dispersion curves of the Stoneley waves in an elastic multilayered medium can therefore be obtained [30]. The characteristic equation shows that the phase velocity of Stoneley interface waves is a function of the material properties (density and Lamé constants), the geometric parameters (thickness) of the different layers and the wave number.

## 2 AE Wave Propagation in Plates

Acoustic emission in plates exhibits some specificities relatively to bulk media. The basic point of interest is the fact that wave propagation is by definition dispersive as already explained in the first part of the chapter. The consequence is that the waves will propagate on different velocities depending on their frequency, see for example the dispersion curves of Fig. 4 which clearly depicts an example of the function of phase velocity over frequency. This also implies that the shape of the waveform will change as one pulse will practically include a bandwidth of frequencies, with the different components traveling on a different speed. This essentially means that the pulse will become elongated with propagation. In bulk media, wave dispersion is also noticed, but not due to geometry. The origin in that case is the heterogeneity which results in scattering [31]. The effect of scattering dispersion is such that the phase velocity in a heterogeneous medium (concrete for instance) may change by 10–15% with an increase in frequency from 20 to 500 kHz, as seen for example in [32, 33]. However, the effect of plate geometry is much stronger as seen above, imposing even cut-off frequencies below which specific wave modes do not propagate. It is reasonable that the two types of dispersion (due to plate waves and scattering) may well co-exist in the case of heterogeneous plates.



Apart from the wave propagation itself, the influence of the excitation is strong. The different possible orientations of the sources play a role in the acquired waveform. Simply, a crack propagating vertical to the axis of the plate structure results in much different waveform than a crack in the parallel direction, as will be shown. The reason is the different proportion of “symmetric” and “antisymmetric” wave modes excited [34, 35]. Plate structures when made by composite laminates may suffer from delaminations which are defects parallel to the plate. When they open (Fig. 5a), their motion is perpendicular to the plate axis and therefore, the excited wave contains much stronger antisymmetric components. On the contrary, when a vertical crack opens (Fig. 5b), this gives rise mainly to symmetric waves having different propagation velocities as has been shown above for most of the range of frequencies until they fall on the Rayleigh wave velocity. Certainly, this is a consideration receiving stochastic nature taking into account the possible orientations as well as the exact point of the crack opening in addition to the heterogeneity of the medium but it is backed up by many researchers in literature occupying with the characterization of the fracture modes in plate structures [36–39].

To indicate the influence of the different specificities in AE plate monitoring, some indicative simulations are presented below. These illustrate the strong difference that the source and geometry can make on the AE waveform showing at the same time the influence of propagation distance in plate geometry compared to three-dimensional media. Examined parameters are:

- (A) the thickness of the plate (essentially thin plate vs. bulk block)
- (B) orientation of the source: horizontal (simulating delamination in layered media) or vertical crack
- (C) the position of the source in terms of thickness (e.g. mid-thickness or surface breaking) and
- (D) the distance between source and receiver, which is not examined separately but in parallel with the above-mentioned parameters due to multiple sensor placement.

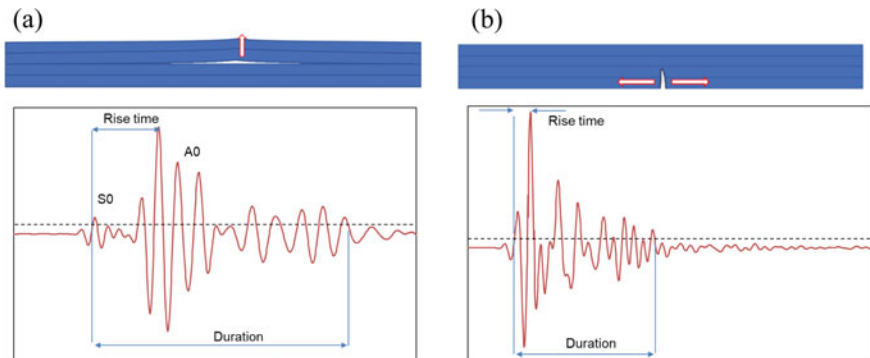


**Fig. 5** Schematic representation of damage event in plate with typical AE waveform: left, horizontal crack (delamination), right, vertical (matrix) crack

Let us go through these parameters in detail:

- (A) Thickness of the plate or essentially difference between plate and surface waves

It is interesting to first demonstrate an example of plate wave propagation compared to the propagation in a bulk medium, while other conditions, like material properties, excitation, sensor distance remain the same. For the case of plate, the indicative geometry is 1 m long with 5 mm thickness. Three receivers are placed on the top side, with a separation distance of 300 mm between them (see Fig. 6a). A fourth receiver is placed at the bottom, beneath the third sensor, having thus the same distance from the source (620 mm) but on the opposite side. Their size is 1 mm and the outcome, is the averaging of the vertical displacement on their size. This size is deliberately small to resemble more the ideal “point” receiver and minimize “aperture effects” that are discussed in chapter “Sensors and Instruments”. The excitation, is placed 20 mm to the right of the first receiver and simulates initially a horizontal crack (could be delamination in a composite) of 1 mm in the central part of the thickness of the beam, meaning that the excitation motion has the direction vertical to the axis of the plate. It consists of one cycle of 100 kHz (10  $\mu$ s duration). Infinite medium boundary conditions are applied on the left and right sides while the space

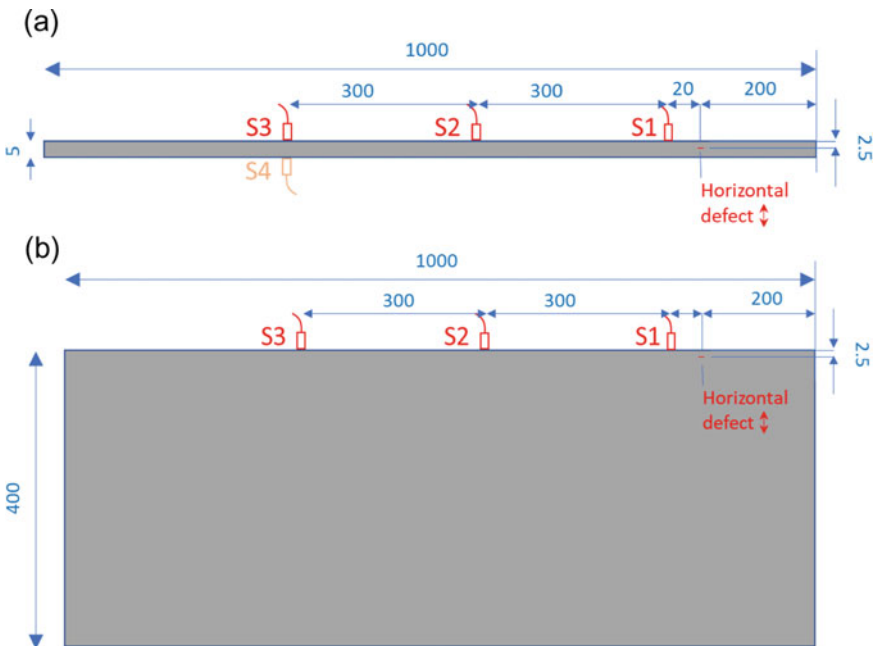
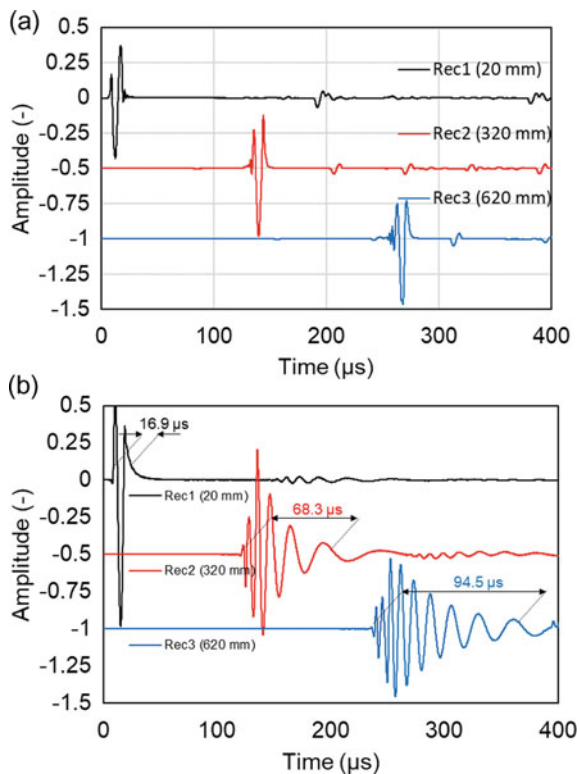


**Fig. 6** Schematic representation of the geometric numerical models. The vertical red arrow at the horizontal defect indicates the motion direction, **a** thin plate, **b** thick geometry. Dimensions are in mm

resolution is 0.1 mm. In order to highlight the effect of the plate wave dispersion on the received waveforms, the corresponding simulation on a bulk medium is also presented for the necessary comparison. The top side of the bulk geometry (including receivers, excitation) and the material properties are maintained as above, while the thickness becomes 400 mm, in order to depart from the thin plate concept (see Fig. 6b). The material in both cases was considered homogeneous with a longitudinal wave velocity of 4200 m/s, corresponding to a longitudinal wavelength of 42 mm for the selected frequency. This is much longer than the thickness of the plate (5 mm) clearly resulting in Lamb waves for the thin case. On the other hand, it is much lower than the thickness in the case of bulk medium (400 mm) allowing therefore, pure Rayleigh waves with speed of approximately 2300 m/s and wavelength (and thus penetration depth) of 23 mm, without plate influence.

Below, in Fig. 7a one can see the waveforms of the three receivers for the bulk (thick) medium first which is considered as reference. The main part of the signal consists of one main cycle, while small reflections from the bottom boundary can also be observed after the main cycle. It is evident that the shape of the pulse does not significantly change during the propagation resembling the initial form of a single cycle. This is due to the aforementioned non-dispersive nature of Rayleigh waves

**Fig. 7** Simulated waveforms for the case of **a** thick medium, **b** thin plate after vertical excitation (simulating delamination) of 1 cycle of 100 kHz



(like longitudinal and shear waves). It is mentioned that there is a small part of longitudinal waves ahead of the Rayleigh but its amplitude is negligible and cannot be clearly discerned in this scale.

In Fig. 7b the responses for the case of thin plate are depicted. Here, it is obvious that the waveform changes with longer propagation. The second receiver's waveform contains several cycles while the third waveform is even longer. In addition, it is quite obvious that the signal starts with shorter cycles (higher frequency) while longer cycles follow, showing vividly the effect of dispersion, or else the dependence of wave speed on frequency. Looking at the waveform from the perspective of AE, all parameters change depending on the distance. Indicatively, the horizontal source (delamination) which is studied herein, will have an AE signature of 1 cycle if monitored 20 mm away (Rec. 1, 20 mm in Fig. 7b), but if the sensor is approximately 600 mm away, the main signal consists of approximately ten cycles. This will already result in serious change in the duration, the RT, the average frequency, the whole frequency spectrum and any parameter used for damage classification in AE. For an indicative fixed threshold of 5% of the maximum response of the 1st sensor, the duration of the signal will change from 16.9  $\mu\text{s}$  for the nearby sensor, to 68.3  $\mu\text{s}$  for the 2nd and to 94.5  $\mu\text{s}$  for the last sensor, despite the same excitation of one cycle (of duration 10  $\mu\text{s}$ , or RT of 2.5  $\mu\text{s}$ ). This is the reason that especially in plates, a certain acoustic signature cannot be directly assigned to a specific failure mechanism. In any case, consideration of the distance is crucial.

#### (B) Excitation direction

Now let us change the direction of excitation and simulate a matrix crack located vertical in the plate as in Fig. 8.

The resulting waveforms are shown in Fig. 9. Comparing with the previous case of delamination (Fig. 7b), the main part of the wave seems much shorter as it consists of one basic cycle, followed by weaker arrivals. It is also observed that the wave is recorded much earlier than the case of delamination. Indicatively, the first disturbance at the last receiver (at 620 mm) arrives just before 150  $\mu\text{s}$ , while for the delamination case shown in Fig. 7b above, the waveform essentially started at 235  $\mu\text{s}$ . This is indicative of the different wave modes excited: in the case of vertical defect (matrix crack) the dominant mode is the fast symmetric, while for the horizontal defect (delamination) this is the slower antisymmetric.

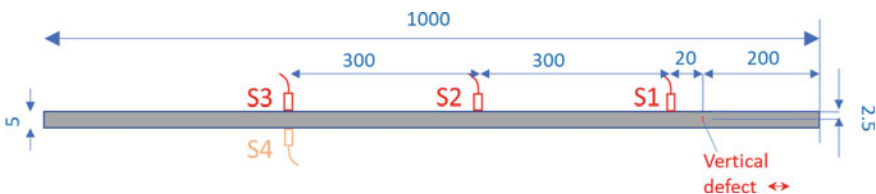


**Fig. 8** Schematic representation of the geometric numerical model of a plate with a vertical source (crack). The horizontal arrow at the vertical defect indicates the motion direction. Dimensions are in mm

**Fig. 9** Simulated waveforms for the case of thin plate after horizontal excitation (simulating vertical crack in the middle of the thickness) of 1 cycle of 100 kHz

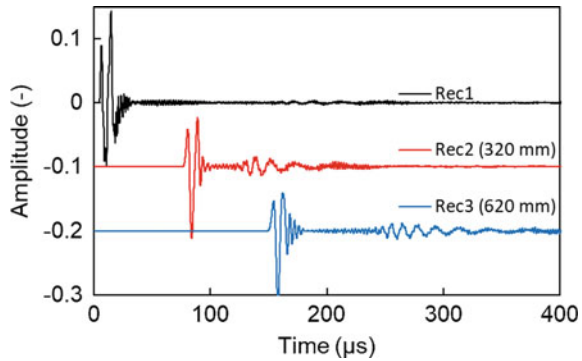
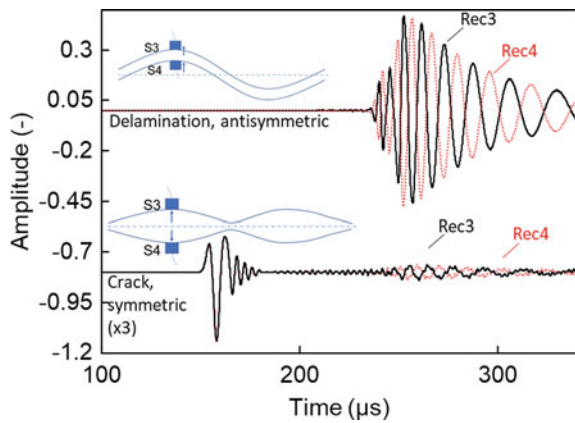


**Fig. 10** Simulated waveforms on the plate geometry for opposite facing sensors S3 and S4 after horizontal delamination and vertical crack excitation

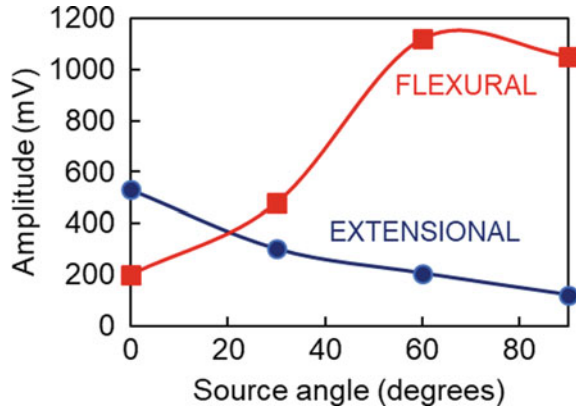


To demonstrate another difference between the modes, the responses of the furthest receiver (#3) for both cases are placed together in Fig. 10 in addition with the responses of receiver #4 which is placed on the exact opposite point, below #3.

In the first case of simulated delamination (Fig. 10 top), the two sensors obtain waveforms with opposite phase, meaning that when receiver #3 shows a positive peak, receiver #4 shows negative and vice versa. This is indicative of the antisymmetric mode, as the top and bottom sensors are placed on opposite surfaces, facing each other. Therefore, an upwards motion on the plate, is felt as compressional from the top sensor but tractional from the bottom sensor. On the other hand, when a vertical crack is active (see bottom part of Fig. 10), this results in a symmetric mode and the sensors record essentially the same waveform. This is a way to identify the different contributions even in case where the waveform contains mixed modes. By subtracting the response of the two sensors, the symmetric component mode is eliminated, and the remaining part corresponds to the antisymmetric one.

In any case, as evident by comparing the waveforms of the same sensor (example S3) for different excitations (horizontal or vertical defect), the received signal shows

**Fig. 11** Amplitude of two plate wave modes on a metal plate, relatively to the orientation of excitation ( $0^\circ$  denotes parallel to the plate). Data taken from [40]



strong dependence on the orientation of excitation, enabling thus the effort to characterize the damage mode (delamination or matrix crack) based on the sensor response. An early experimental work [40] dealing with this issue was conducted on metal plate geometry and through notches, excitations at different angles were performed. Apart from the out-of-plane ( $90^\circ$ ) and the in-plane ( $0^\circ$ , same direction with the plate axis), two other excitation angles ( $30^\circ$  and  $60^\circ$ ) were examined, showing the gradual shift of the content from the fast symmetric wave (called extensional) to the slower anti-symmetric (called flexural), as measured by an ultrasonic transducer with relatively flat response between 20 kHz and 1 MHz, placed on the surface of the plate. Figure 11 represents the data from this study clearly showing the dependence of the extensional and flexural mode on the orientation exactly as the above discussed simulations.

### (C) Position of excitation

In the above cases of totally central excitation the produced wave is almost purely symmetric (vertical crack) or antisymmetric (horizontal delamination) as seen by the output of sensors of Figs. 7b and 9. However, when the source does not come exactly from the mid-thickness this results in a mixed mode. Let us indicatively examine the effect of position of the excitation as in a real plate the source will not necessarily be exactly in the mid-thickness.

Figure 12a shows the waveforms for the case of a vertical crack which is surface breaking at the bottom with a length of 1 mm, shown in Fig. 12b. The geometric model is the same as described above in Fig. 8 with the only difference that the crack is not located in the mid-thickness, but 2 mm lower, thus breaking the bottom surface. It is again seen that the response of receiver 1 does not exhibit strong changes for the different excitation patterns because of the limited distance to the source. Indeed, a minimum propagation distance of more than 5 times the thickness is considered enough to form distinct Lamb modes [41]. Receivers 2 and 3, clearly record both modes, the symmetric that comes at approximately  $150 \mu\text{s}$  at receiver 3 (like in the case of central crack in Fig. 9) and at the same time the antisymmetric after  $200 \mu\text{s}$ . Certainly the amplitude of both modes is decreased compared to the previous figures

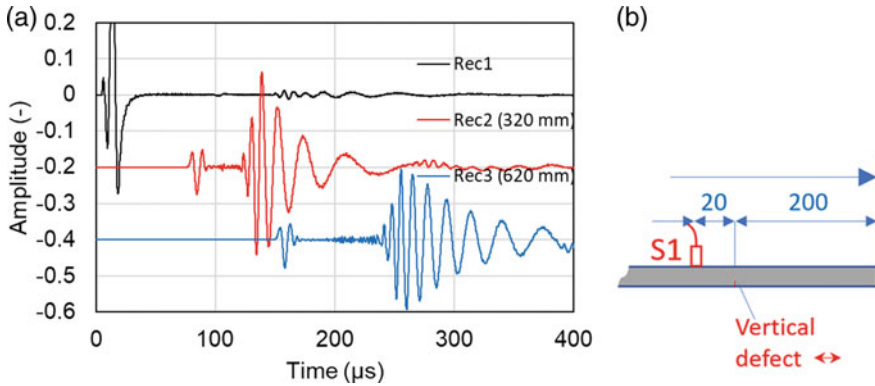


**Fig. 12** **a** Simulated waveforms for the case of thin plate after horizontal excitation (simulating vertical surface breaking crack at the bottom) of 1 cycle of 100 kHz. **b** Detail of the source location (surface breaking crack)

as the excitation energy is distributed in two modes rather than one. Similar trends in experimental results have been shown in the past using pencil lead break excitations at different depths in a steel bar of 12 mm thickness. The gravity of the waveform strongly shifted just by moving the excitation a few mm from top to the middle of the plate [42].

The influence of the width of the plate structure was examined in metal [43] and composite plates [44]. Large plates are less influenced by reflections, while the wave energy is dispersed to larger areas compared to a less wide plate (or beam). This has a serious effect on the recorded wave after the same excitation, as demonstrated on metals and cementitious composite specimens. Specifically, after pencil lead break excitation on beam and plate geometries of the same material (see geometries in Fig. 13a), sensors on beams recorded much higher amplitude for out-of-plane excitations and especially for in-plane ones. The voltage was approximately 5 times higher while the RT was considerably lower as seen in Fig. 13b. At the same time, and as measured by resonant sensors at 150 kHz, although there was not an impressive shift of frequencies, the beam specimen did register a slightly higher peak frequency 145 kHz versus 157 kHz.

Therefore, using a standard source, the differences are obvious between narrow (beams) and wide specimens (plates). However, in an actual fracture event, the source is not the same in a plate and a beam. In the beam case, the crack propagation increment is restricted by the boundaries of the beam, while in a plate this restriction is essentially removed meaning that the released energy may be much higher. At the same time the crack tip in the case of plate may be further away from the sensor, therefore making the predictions on the expected energy quite complicated. Actual AE results in plate and beam specimens of the same material during the early stages of four point bending testing (focusing thus in cracking rather than delaminations) showed similar trends with pencil lead excitations for most of the AE descriptors; indicatively lower RT for the beam (14  $\mu\text{s}$  vs. 46  $\mu\text{s}$  for plate), and higher frequency

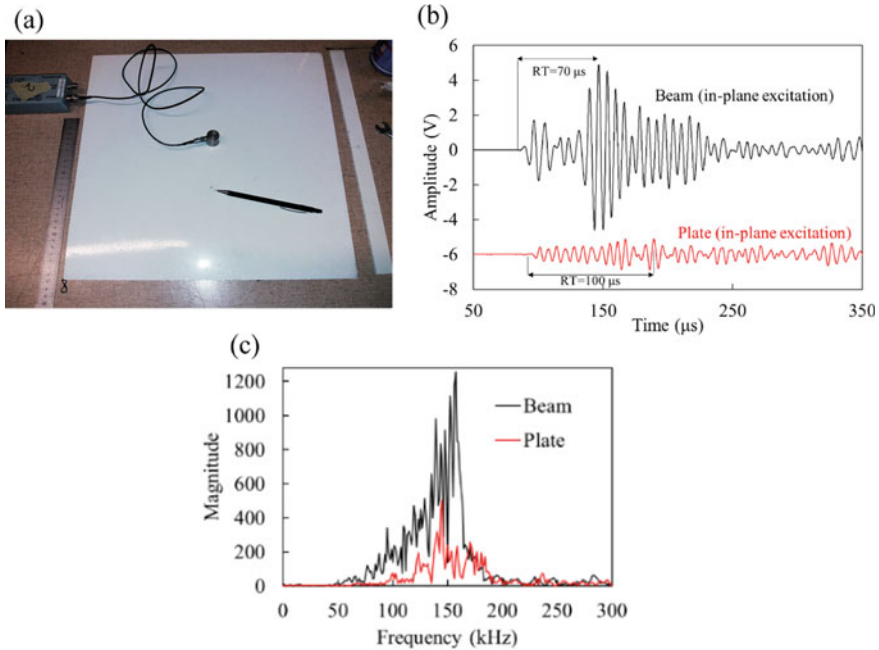


**Fig. 13** **a** Plate (left) and beam specimen (right), **b** waveforms received after pencil lead excitation on the side of the specimens (in-plane excitation) for beam and plate geometries, **c** corresponding FFTs, data from [44]

descriptors for the beam (170 kHz vs. 137 kHz for plate). Indicative waveforms are also shown in Fig. 14 for plate and beam specimens from [44]. The only difference came from the energy related parameters where plate specimens exhibited more than 4 dB stronger amplitude for plate, most likely because of the larger longitudinal dimension of cracks in the plate. In any case, the effect of the plate dimensions is crucial and would not allow to extrapolate the results from a laboratory scale sample to an actual plate. Therefore, the enlargement of laboratory coupons to resemble plates instead of beams is desirable [43].

It is seen therefore, that the type or “mode” of damage although important, is not the unique factor affecting the waveform shape, but its position and the geometry may influence the recorded signal as well. It is also understandable that the possible cases to be examined are infinite. Namely, different angles of cracks and excitations, different number of excitation cycles and central frequency, material properties, layered geometry, existing damage imposing scattering and deterioration of mechanical properties, plate dimensions. However, this chapter aims only to point out the issues arising from the plate geometry and not to exhaust the analysis of all cases, which are essentially infinite. A separate issue is related to the aperture effect, or the interaction between the physical size of the sensor and the wave length, but this is treated in the chapter “[Sensors and Instruments](#)”.



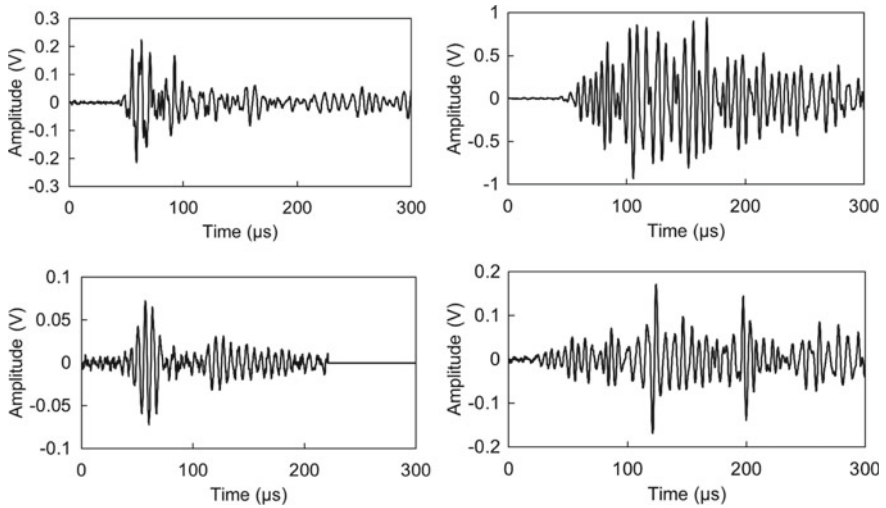


Fig. 14 Typical AE signals during cracking in beam (left) and plate (right) TRC specimens

### 3 Examples of AE Application in Plates

AE is casually used for assessment of plate geometries. The above-mentioned effects of wave distortion due to dispersion may complicate the characterization in some cases, especially when detailed analysis is attempted, however, by no means hinder the application of AE in numerous applications in laboratory and industrial practice. Below lie several applications of AE in plate structures, highlighting at the same time these effects.

Figure 15a shows a photograph of AE test during bending loading of a thin textile reinforced cement (TRC) specimen taken from [38]. In this case four sensors were

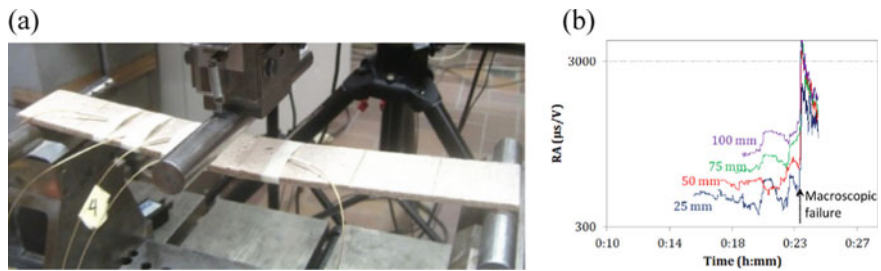


Fig. 15 a Photograph of three-point bending of TRC beam with concurrent AE monitoring by sensors at different distances from the center, b AF history vs. time for sensors at different distances from the damaged area [38]

placed at distance intervals of 25 mm between them. Looking at specific AE parameters like the RA value in Fig. 15b, the moment of shift between successive fracture mechanism (in this case between matrix cracking and delamination) is clearly pointed out. It is reminded, that as explained in chapter “[Parametric AE Analysis](#)” RA is the ratio of the rise time of the waveform over the amplitude and is measured in  $\mu\text{s}/\text{V}$ . The RA, as monitored by the closest sensor at 25 mm from the main fracture area fluctuates around  $400 \mu\text{s}/\text{V}$  during matrix cracking and increases to more than  $3000 \mu\text{s}/\text{V}$  when the dominant mode shifts to delaminations. Monitoring by any other sensor clearly shows the transition as well. However, the interesting point, which also reveals the influence of the propagation on the plate geometry is that the different sensors received the same damage events with different AE characteristics depending on the distance from the main damage zone. Specifically the curve of the furthest away sensor at 100 mm is situated much higher at approximately  $1000 \mu\text{s}/\text{V}$ . Even after the main failure when cracks are saturated and delaminations dominate, there is still a difference with the closer sensor indicating lower RA than the furthest. This result and many similar others in the recent literature indicate, as will be seen, that care should be taken when fracture mode characterization is attempted, since the propagation distance influences the readings of the sensors.

The decrease of frequency and increase of RA of cracking signals render them more like shear signals emitted close to the sensor and therefore, make the inclusion of propagation distance necessary in any analysis [45]. In a numerical study concerning homogeneous medium (metal) [46] the change of AE parameters after a simulated cracking event in a homogeneous plate was considered using multiple receivers on the surface. Apart from the fact that waveform shape change was obvious, the RT and RA monotonically increased with distance up to 500 mm (as seen in Fig. 16) for any of the simulated frequencies (500 kHz to 2 MHz). Peak amplitude on the other hand dropped while the only parameter not much affected was the frequency content expressed by the frequency centroid after FFT, more likely because no damping was included in the model for the steel material. Due to the monotonic shift of AE parameters with distance a “correction” methodology was proposed to evaluate the original values of the waveform at the source [46].

Similar indications were given from a numerical study, which among many other parameters, studied also the effect of propagation distance on a steel plate of 3 mm [47] considering distances between 25 and 200 mm. The extensive waveform shape change was attributed to the velocity difference between S0 and A0, with the latter strongly contributing in the sensors close to excitation, while for the more distant ones, the A0 contribution arrive much later due to dispersion.

Continuing this small journey over waveform distortion, these trends are seen in [34] where the “weight” of the signals emitted either from matrix cracking or delamination is obviously translated to different parts of the waveform for different sensor locations. This effect renders characterization of the source not straightforward as propagation needs to be accounted for.

Other examples of parameters change due to propagation are briefly shown below in indicative materials. In [48] where carbon fiber reinforced polymer composites are monitored, the frequency centroid of AE signals due to internal cracks lost about

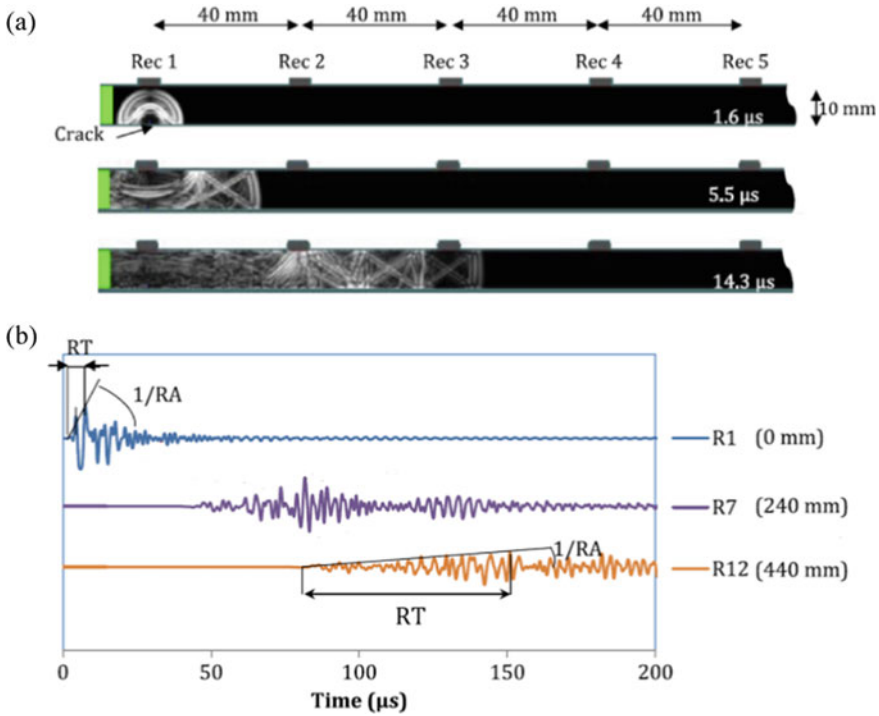


**Fig. 16** **a** Simulated strain field on a metal plate cross section at different times after the occurrence of the excitation of 2 MHz, **b** simulated waveforms collected from successive sensors at the top of the specimen

300 kHz while propagating a maximum distance of 80 mm (from an average of 800–500 kHz). In [49] discrimination of the source of damage in carbon fiber composites is attempted based, among others, on the amplitude of the S0 and A0 modes which are characteristic of in-plane damage (cracking) and out-of-plane (delaminations). However, the effect of attenuation is dissimilar for the two wave modes and therefore, a correction procedure is applied depending on the propagation distance of each wave. The “corrected” amplitude ratio of the two modes is then fed into a pattern recognition algorithm to end up to the final classification [50].

In an earlier application AE in composite (graphite/epoxy) plates under impact was studied. Penetrating impact caused naturally higher amplitudes of AE waveforms than non penetrating. However, an interesting phenomenon was observed in that the large flexural mode component, seen in any other case, was absent from the signal when the impact particle fully penetrated through the composite plates [51].

Several examples of AE analysis in composites are also discussed in the chapter “Parameter-based AE Analysis”. An example of 2D (planar) localization is shown in Fig. 17a. The event density distribution on the floor of a corroded storage tank (Fig. 17b) is depicted [52]. Active corrosion processes cause acoustic emission, which

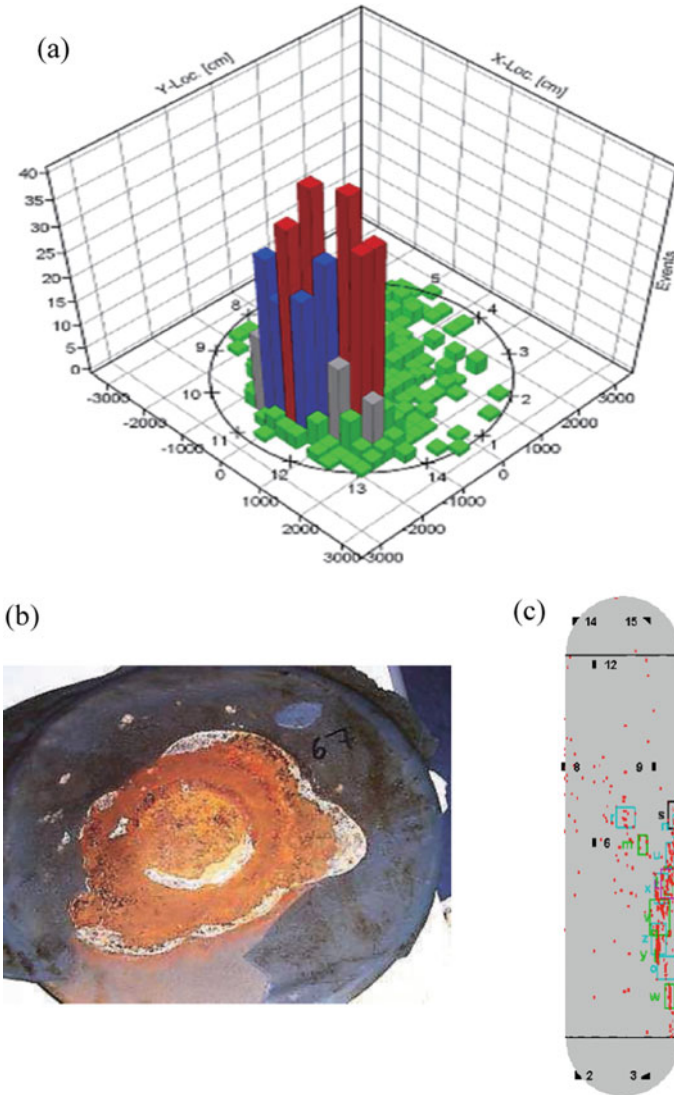


**Fig. 17** a AE planar localization, b in corroded storage tank bottom [52], c localization in cylindrical composite petrochemical tank [54]

can be monitored and mapped during testing. The monitoring takes place normally during operation without the need to empty and clean the tank for visual inspection. Similar results were exhibited in [53], where the location of AE events coincided with reduced thickness due to corrosion in a tank bottom.

Another example of industrial application of AE localization in curved thin metal plates is demonstrated in Fig. 17c. The roughly 8 m long structure operates under

high internal pressure and temperature. Therefore, a cool down process is followed, during which thermal gradients are developed through the wall. These give rise to thermal strains in addition to mechanical ones and any growing discontinuities can be detected by AE sensors located around the vessel. In the present case, certain areas with high density of flaws (sources of red color) are identified and further examination is due after removing the insulation layer [54].

The effect of repair or healing on textile reinforced cement plate was evident through AE in [55]. Plates that were thermally precracked exhibited a more wide distribution of cracking away of the central loading point. At the same time they exhibited more “shear” AE characteristics (higher rise time, duration, lower frequency) since cracking had already been saturated due to thermal treatment and damage continued with fiber pull-out and delaminations. Plates that contained self-healing agent and were treated in high temperatures to activate it, exhibited AE parameters closer to the intact laminate, meaning that the cracking mechanism was again activated and showing the effectiveness of healing along with pulse velocity and attenuation measurements [55].

Localization may of course be impacted by erroneous results due to different velocities of the wave modes [40], but in general, as also some examples above demonstrate, AE localization works quite well and provides reasonable engineering accuracy in plates. However, at some points Lamb waves even create opportunities like the localization by less sensors than normally required from the dimensions of the geometry. Although it is typically required to have multiple sensors for localization purposes it is possible to apply localization in certain structures using only one sensor. Specifically, in plate geometries linear localization approaches using only one sensor have been proposed, taking advantage of the time delay between different Lamb wave modes [56, 57]. These modes obtain different velocities and therefore, the further away they propagate, the longer the delay between the fast symmetric and the slower antisymmetric becomes. By knowing the elastic properties of the plate, the velocities of the wave modes are calculated and consequently their time lag is translated to propagating distance. The same mentality has been extended in 2D localization using only two sensors in composite plates [58, 59]. A phenomenological paradox is seen therefore; although plate wave dispersion may pose difficulties in many cases in the identification of the received components, in other cases it enables localization by less sensors than normally required! It depends on the mentality and the focus of each experiment.

The limits may be pushed further, and this basically concerns slight improvements and special cases (e.g. geometries with holes) as already results are considered satisfactory either in laboratory or large scale.

## 4 Conclusions

Plate geometries are common in load-bearing engineering structures. AE in plate structures presents some specificities compared to bulk media. These concern the

plate waves and the associated dispersion which are activated when the wave length starts to become of the same order with the thickness. Different modes are observed, propagating at different speeds being also influenced by the frequency. Therefore, the AE waveform shape changes. Basic features of AE testing like localization and parameter analysis are very successful in plates, however, care shall be taken when quantitative characteristics are to be analyzed. This is because energy-related and waveform-related parameters strongly depend on the frequency as well as the propagation path. While characterization produces accurate engineering results as demonstrated in various applications in different matrix composites and metals, the limits could be further pushed in fracture mode determination by improving the interpretation of the AE parameters and isolate the source effect from the propagation effect.

## References

1. Rösner H, Meyendorf N, Sathish S, Matikas TE (2000) Nondestructive evaluation of fatigue in titanium alloys. *MRS* 591:73–78
2. Sathish S, Martin SW, Matikas TE (1999) Rayleigh wave velocity mapping using scanning acoustic microscope. In: *Proceedings of review of progress in quantitative nondestructive evaluation*, vol 18. Plenum, New York, pp 2025–2030
3. Sathish S, Matikas TE, Stryker A, Nagy PB (2000) Acoustic techniques for early detection of fatigue damage. In: *Proceedings of AeroMat*, Dayton, Ohio
4. Aggelis DG, Kordatos EZ, Strantza M, Soulioti DV, Matikas TE (2011) NDT approach for characterization of subsurface cracks in concrete. *Constr Build Mater* 25(7):3089–3097
5. Daponte P, Maceri F, Olivito RS (1995) Ultrasonic signal-processing techniques for the measurement of damage growth in structural materials. *IEEE Trans Instrum Meas* 44(6):1003–1008
6. Dassios KG, Matikas TE (2013) Damage assessment in a SiC-fiber reinforced ceramic matrix composite. *J Eng* 2013:6. Published online
7. Viktorov IA (1967) *Rayleigh and lamb waves*. Plenum Press, New York
8. Viktorov IA (1967) *Rayleigh and lamb waves: physical theory and applications*. Plenum Press
9. Matikas TE, Shell E, Nicolaou PD (1999) Characterization of fretting fatigue damage using nondestructive approaches. In: *Proceedings of SPIE conference on nondestructive evaluation of aging materials and composites III*, vol 3585, pp 2–10, 0277786X (ISSN). SPIE—The International Society for Optical Engineering, Newport Beach, CA, USA. <https://doi.org/10.1117/12.339835>
10. Bar-Cohen Y, Lih SS, Mal AK (2001) NDE of composites using leaking lamb waves. *NDT&E J*
11. Diamanti K, Hodgkinson JM, Soutis C (2002) Damage detection of composite laminates using PZT generated lamb waves. In: Balageas D (ed) *Structural health monitoring*. DESTech Publications Inc., pp 398–405
12. Light GM, Minachi A, Spinks RL (2001) Development of a guided wave technique to detect defects in thin steel plates prior to stamping. In: *Proceedings of 7th ASME NDE topical conference*, vol 20, pp 163–165
13. Lin X, Yuan FG (2001) Damage detection of a plate using migration technique. *J Intell Mater Syst Struct* 12(7)
14. Mal A (2001) NDE for health monitoring of aircraft and aerospace structures. In: *Proceedings of 7th ASME NDE topical conference*, vol 20, pp 149–155

15. Devilla F, Roldan E, Tirano C, Mares R, Nazarian S, Osegueda R (2001) Defect detection in thin plates using S0 lamb wave scanning. In: Proceedings of SPIE advanced nondestructive evaluation for structural and biological health monitoring, vol 4335, pp 121–130
16. Duke JC (1988) Acousto-ultrasonics—theory and applications. Plenum Press
17. Dupont M, Osmont R, Gouyon R, Balageas DL (2000) Permanent monitoring of damage impacts by a piezoelectric sensor based integrated system. In: Chang F-K (ed) Structural health. Technomic, pp 561–570
18. Benson DM, Karpur P, Matikas TE, Kundu T (1995) Experimental generation of lamb wave dispersion using Fourier analysis of leaky modes. In: Proceedings of 21th annual review of progress in quantitative nondestructive evaluation, vol 14A. Plenum, New York, Snowmass Village, Colorado, pp 187–194
19. Benson DM, Karpur P, Stubbs DA, Matikas TE (1995) Characterization of damage progression and its correlation to residual strength in a sigma/Ti-6242 composite using nondestructive methods. ASME (Eng Mater) 69(1):285–292
20. Krishnamurthy S, Matikas TE, Karpur P, Miracle DB (1995) Ultrasonic evaluation of the processing of fiber-reinforced metal-matrix composites. Compos Sci Technol 54(2):161–168
21. Krishnamurthy S, Matikas TE, Karpur P, Miracle DB (1995) Ultrasonic techniques for the interface characterization of continuously reinforced metallic composites. In: Proceedings of TMS/ASM symposium on interface measurements and application to MMC properties, Cleveland, Ohio
22. Kundu T, Ehasni M, Maslov KI, Guo D (1999) C-scan and L-scan generated images of the concrete/GFRP composite interface. NDT&E Int 32(2):61–69
23. Kundu T, Karpur P, Matikas TE, Nicolaou PD (1996) Lamb wave mode sensitivity to detect various material defects in multilayered composite plates. In: Proceedings of 22th review of progress in quantitative nondestructive evaluation, vol 15A. Plenum, New York, Seattle, Washington, pp 231–238
24. Kundu T, Maslov K, Karpur P, Matikas TE, Nicolaou PD (1996) A lamb wave scanning approach for the mapping of defects in [0/90] titanium matrix composites. Ultrasonics 34(1):43–49
25. Hu C, Yang B, Xuan F-Z, Yan J, Xiang Y (2020) Damage orientation and depth effect on the guided wave propagation behavior in 30CrMo steel curved plates. Sensors (Switzerland) 20(3), art. no. 849
26. Liu H, Yang JL, Liiu KX (2007) Love waves in layered graded composite structures with imperfectly bonded interface. Chin J Aeronaut 20(3):210–214
27. Barnett DM, Lothe J, Gavazza SD, Musgrave MJ (1985) Considerations of the existence of interfacial (Stoneley) waves in bonded anisotropic elastic half-spaces. Proc R Soc Lond A402:153–166
28. Tomar SK (2006) Propagation of Stoneley waves at an interface between two microstretch elastic half-spaces. J Vib Control 12(9):995–1009
29. Zhu J, Popovics JS, Schubert F (2004) Leaky Rayleigh and Scholte waves at the fluid-solid interface subjected to transient point loading. J Acoust Soc Am 116(4):2101–2110
30. Li B, Li M-H, Tong Lu (2018) Interface waves in multilayered plates. J Acoust Soc Am 143(4):2541–2553
31. Graff K (ed) (1991) Scattering and diffraction on elastic waves. Wave motion in elastic solids. Dover Publications, pp 394–430 (Chap. 7)
32. Chaix JF, Garnier V, Corneloup G (2006) Ultrasonic wave propagation in heterogeneous solid media: theoretical analysis and experimental validation. Ultrasonics 44:200–210
33. Philippidis TP, Aggelis DG (2005) Experimental study of wave dispersion and attenuation in concrete. Ultrasonics 43(7):584–595
34. Scholey JJ, Wilcox PD, Wisnom MR, Friswell MI (2010) Quantitative experimental measurements of matrix cracking and delamination using acoustic emission. Compos A 41:612–623
35. Eaton M, May M, Featherston C, Holford K, Hallet S, Pullin R (2011) Characterisation of damage in composite structures using acoustic emission. J Phys Conf Ser 305:012086



36. Sause M, Hamstad M (2018) 7.14 acoustic emission analysis. In: Beaumont PWR, Zweben CH (eds) *Comprehensive composite materials II*, vol 7. Academic Press, Oxford, pp 291–326
37. Li L, Lomov SV, Yan X (2015) Correlation of acoustic emission with optically observed damage in a glass/epoxy woven laminate under tensile loading. *Compos Struct* 123:45–53
38. Blom J, El Kadi M, Wastiels J, Aggelis DG (2014) Bending fracture of textile reinforced cement laminates monitored by acoustic emission: influence of aspect ratio. *Constr Build Mater* 70:370–378
39. Kolanu NR, Raju G, Ramji M (2019) Damage assessment studies in CFRP composite laminate with cut-out subjected to in-plane shear loading. *Compos Part B Eng* 166:257–271
40. Gorman MR, Prosser WH (1991) AE source orientation by plate wave analysis. *J Acoust Emiss* 9(4):283–288
41. Hamstad MA (2007) Lamb modal regions with significant AE energy in a thick steel plate. In: *International conference on acoustic emission—advances in acoustic emission*, pp 247–252
42. Dunegan HL (1996) The use of plate wave analysis in acoustic emission testing to detect and measure crack growth in noisy environments. In: *Structural materials technology NDE conference*, San Diego, CA, Feb 1996. <https://trid.trb.org/view/464284>. Accessed March 2021
43. Hamstad MA, O’Gallagher A, Gary J (2001) Effects of lateral plate dimensions on acoustic emission signals from dipole sources. *J Acoust Emiss* 19:258–274
44. Ospitia N, Aggelis D, Tsangouri E (2020) Dimension effects on the acoustic behavior of trc plates. *Materials* 13(4). Art. no. 0955
45. Aggelis DG, El Kadi M, Tysmans T, Blom J (2017) Effect of propagation distance on acoustic emission fracture mode classification in textile reinforced cement. *Constr Build Mater* 152:872–879
46. Aggelis DG, Matikas TE (2012) Effect of plate wave dispersion on the acoustic emission parameters in metals. *Comput Struct* 98–99:17–22
47. Sause MGR, Hamstad MA (2018) Numerical modeling of existing acoustic emission sensor absolute calibration approaches. *Sens Actuators A Phys* 269:294–307
48. Mailliet E, Baker C, Morscher GN, Pujar VV, Lemanski JR (2015) Feasibility and limitations of damage identification in composite materials using acoustic emission. *Compos A Appl Sci Manuf* 75:77–83
49. McCrory JP, Al-Jumaili SKh, Crivelli D, Pearson MR, Eaton MJ, Featherston CA, Guagliano M, Holford KM, Pullin R (2015) Damage classification in carbon fibre composites using acoustic emission: a comparison of three techniques. *Compos Part B* 68:424–430
50. Al-Jumaili SKh, Holford KM, Eaton MJ, Pullin R (2015) Parameter correction technique (PCT): a novel method for acoustic emission characterisation in large-scale composites. *Compos Part B* 75:336–344
51. Prosser WH, Gorman MR, Humes DH (1999) Acoustic emission signals in thin plates produced by impact damage. *J Acoust Emiss* 17(1–2):29–36
52. Teschliesnig P, Jagenbrein A, Lackner G (2016) Corrosion detection for ferritic structures. In: JSNDI & IIIAE (eds) *Progress in acoustic emission XVIII*, Shiotani, Wakayama, Enoki, Yuyama, pp 43–48
53. Takemoto M, Cho H, Suzuki H (2006) Lamb-wave acoustic emission for condition monitoring of tank bottom plates. *J Acoust Emiss* 24:12–21
54. Papasalouros D, Bollas K, Kourousis D, Anastasopoulos A (2016) Acoustic emission monitoring of high temperature process vessels & reactors during cool down. In: *Emerging technologies in non-destructive testing VI—proceedings of the 6th international conference on emerging technologies in nondestructive testing, ETNDT 2016*, pp 197–201
55. El Kadi M, Blom J, Wastiels J, Aggelis DG (2017) Use of early acoustic emission to evaluate the structural condition and self-healing performance of textile reinforced cements. *Mech Res Commun* 81:26–31
56. Surgeon M, Wevers M (1999) One sensor linear location of acoustic emission events using plate wave theories. *Mater Sci Eng A* 265:254–261
57. Ebrahimkhanlou A, Salamone S (2017) Acoustic emission source localization in thin metallic plates: a single-sensor approach based on multimodal edge reflections. *Ultrasonics* 78:134–145



58. Toyama N, Koo JH, Oishi R, Enoki M, Kishi T (2001) Two-dimensional AE source location with two sensors in thin CFRP plates. *J Mater Sci Lett* 20(19):1823–1825
59. Aljets D, Chong A, Wilcox S, Holford K (2012) Acoustic emission source location on large plate-like structures using a local triangular sensor array. *Mech Syst Signal Process* 30:91–102